




Anion Coordination into Ligand Clefts

Matteo Savastano ^{1,2,*}, Carlotta Cappanni ¹, Carla Bazzicalupi ^{1,*}, Cristiana Lofrumento ¹
and Antonio Bianchi ¹

¹ Department of Chemistry "Ugo Schiff", University of Florence, Via della Lastruccia, 3-13, 50019 Sesto Fiorentino, Italy; carlotta.cappanni@stud.unifi.it (C.C.); cristiana.lofrumento@unifi.it (C.L.); antonio.bianchi@unifi.it (A.B.)

² National Interuniversity Consortium of Materials Science and Technology (INSTM), 50121 Florence, Italy

* Correspondence: matteo.savastano@unifi.it (M.S.); carla.bazzicalupi@unifi.it (C.B.)

Abstract: A tripodal anion receptor has been obtained by an easy and fast single-reaction synthesis from commercial reagents. The three ligand arms-bearing aromatic groups able to form anion- π interactions define ligand clefts where large anions, such as perchlorate and perrhenate, are included. We report here the synthesis of the ligand, its acid/base properties in an aqueous solution which has been used to direct the synthesis of anion complexes, and the crystal structure of the free ligand and its anion complexes $H_3L(ClO_4)_2 \cdot H_2O$ and $H_3L(ReO_4)_2$.

Keywords: anion complexes; perrhenate; perchlorate; anion- π ; cleft system

1. Introduction

The design and synthesis of receptors for anionic species have attracted the interest of synthetic chemists since the dawn of supramolecular chemistry. Receptors of increasing complexity have been constructed, from simple linear or branched to more complex macrocyclic and macropolycyclic (cage-like) molecules, which have substantially contributed to forming the general concept that, with few exceptions, more structured and preorganized receptors form more stable anion complexes and provide more efficient molecular recognition processes. Indeed, macrocyclic and macropolycyclic molecules have proved to be very efficient anion receptors. Regrettably, they have the drawback that they often require lengthy and onerous synthetic procedures [1–11].

In this paper, we turn our attention toward a receptor that is easily accessible (from a synthetic point of view) and that, despite its open-chain structure, contains preorganized molecular clefts in which anions can be efficiently housed. This receptor (HL, Figure 1) is a tripodal molecule resembling the tetramine tren (tris(2-aminoethyl)amine), whose protonated species are known to form stable complexes with anions [12], but have a more rigid structure caused by the presence of three aromatic groups. HL can be easily prepared via a single-reaction functionalization of the commercial product N1,N1-bis(pyridin-2-ylmethyl)ethane-1,2-diamine with 6-amino-3,4-dihydro-3-methyl-5-nitroso-4-oxo-pyrimidine (Figure 1 and Section 2).

In an acidic solution, HL undergoes protonation forming ammonium groups able to bind anions via electrostatic attraction and the formation of salt bridges (hydrogen bonds between oppositely charged species). In addition, HL can also use its aromatic groups to bind anions via anion- π interactions. In particular, the pyrimidine inserted into the receptor was chosen precisely for this reason: being highly electron-poor, it has a marked tendency to form anion- π interactions, a characteristic confirmed by the crystal structures of several anion complexes with receptors containing this group [13–17]. Moreover, protonated pyridine groups have a non-negligible ability to form anion- π interactions [18–28].

In this paper, we perform a solid-state analysis of the anion-binding characteristics of H_3L^{2+} , the diprotonated form of HL, toward the monocharged tetrahedral ClO_4^- and



Citation: Savastano, M.; Cappanni, C.; Bazzicalupi, C.; Lofrumento, C.; Bianchi, A. Anion Coordination into Ligand Clefts. *Crystals* **2023**, *13*, 823. <https://doi.org/10.3390/cryst13050823>

Academic Editor: Ana M. Garcia-Deibe

Received: 31 March 2023

Revised: 3 May 2023

Accepted: 13 May 2023

Published: 16 May 2023



Copyright: © 2023 by the authors. Licensee MDPI, Basel, Switzerland. This article is an open access article distributed under the terms and conditions of the Creative Commons Attribution (CC BY) license (<https://creativecommons.org/licenses/by/4.0/>).

ReO_4^- anions, observed in the crystal structures of $\text{H}_3\text{L}(\text{ClO}_4)_2 \cdot \text{H}_2\text{O}$ and $\text{H}_3\text{L}(\text{ReO}_4)_2$. These anions were chosen because, in addition to their technological, biomedical, and environmental interest [29–37], they are challenging targets for binding as they have low charge density and poor hydrogen bonding ability [38,39]. Nevertheless, binding and even recognition of these anions was achieved in some cases, yet the receptors used were often more structurally complex and laborious to prepare [38–41].

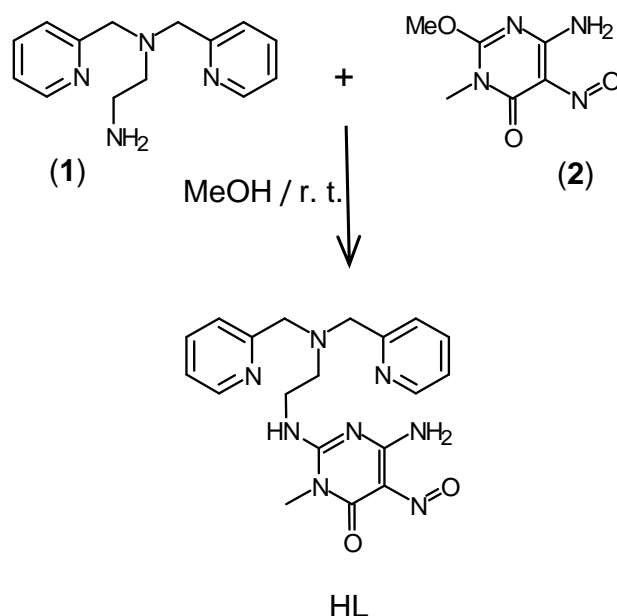


Figure 1. The receptor HL and the schematic procedure for its synthesis.

2. Materials and Methods

2.1. General

All starting materials were high-purity compounds purchased from commercial sources and were used without further purification. Compound 6-amino-3,4-dihydro-3-methyl-2-methoxy-5-nitroso-4-oxopyrimidine (2) was prepared according to a reported procedure [42]. Elemental analysis was performed with a FlashSmart™ Elemental Analyzer (Thermo Fisher Scientific, Monza, Italy).

2.2. Synthesis of HL ($\text{HL} \cdot \text{EtOH} \cdot \text{H}_2\text{O}$)

HL was synthesized as schematically shown in Figure 1. 0.58 g (3.1 mmol) of solid 2 was added in successive portions to a stirred solution of 1 (0.60 g, 2.5 mmol) in methanol (30 cm³) at room temperature. After compound 2 was completely dissolved (about 90 min), 0.5 cm³ of 37% NH_3 was added at room temperature to convert the excess of 2 into the insoluble 2,4-diamino-1-methyl-5-nitroso-6-oxopyrimidine derivative, and the resulting solution was left overnight at 4 °C. The suspension was then filtered and the solution was evaporated to dry under vacuum at room temperature to obtain HL as a deep purple solid compound that was recrystallized from ethanol. Yield 67%. ¹H NMR (D_2O , 400 MHz) δ 8.72 (d, 2H), 8.54 (t, 2H), 8.10 (d, 2H), 7.96 (t, 2H), 4.34 (s, 4H), 3.87 (t, 2H), 3.40 (s, 3H), 3.00 (t, 2H). Anal. calcd. for $\text{C}_{21}\text{H}_{30}\text{N}_8\text{O}_4$ ($\text{HL} \cdot \text{EtOH} \cdot \text{H}_2\text{O}$): C, 55.01; H, 6.59; N, 24.44. Found: C, 54.34; H, 6.52; N, 24.37. The crystals of this sample were suitable for X-ray.

2.3. Synthesis of $\text{H}_3\text{L}(\text{ClO}_4)_2 \cdot \text{H}_2\text{O}$

20 mg (0.044 mmol) of $\text{HL} \cdot \text{EtOH} \cdot \text{H}_2\text{O}$ was dissolved in 5 cm³ of water and the pH of the solution was brought to about 2.5 by the addition of diluted HClO_4 . The crystals of $\text{H}_3\text{L}(\text{ClO}_4)_2 \cdot \text{H}_2\text{O}$ suitable for X-ray analysis were obtained by slow evaporation of this solution at room temperature. The crystals were filtered and air-dried. Yield 47%. Anal. calcd. for $\text{C}_{19}\text{H}_{26}\text{N}_8\text{O}_{11}\text{Cl}_2$: C, 37.21; H, 4.27; N, 18.27. Found: C, 37.09; H, 4.31; N, 18.16.

2.4. Synthesis of $H_3L(ReO_4)_2$

20 mg (0.044 mmol) of $HL \cdot EtOH \cdot H_2O$ was dissolved in 5 cm³ of water and the pH of the solution was brought to about 2.5 by the addition of diluted HCl. A two-fold excess of $NaReO_4$ was then added and the resulting solution was allowed to evaporate at room temperature to form the crystals of $H_3L(ReO_4)_2$ suitable for X-ray analysis. The crystals were filtered and air-dried. Yield 59%. Anal. calcd. for $C_{19}H_{24}N_8O_{10}Re_2$: C, 25.45; H, 2.70; N, 12.49. Found: C, 25.13; H, 2.78; N, 12.41.

2.5. Potentiometric Measurements

Ligand (HL) protonation constants were determined by means of potentiometric (pH-metric) titrations in 0.1 M NMe_4Cl aqueous solution at 298.1 ± 0.1 K using an automated apparatus and a procedure previously described [43]. The acquisition of the emf data was performed with the computer program PASAT [44,45]. The combined electrode (Metrohm 6.0262.100, Metrohm, Herisau, Switzerland) was calibrated as a hydrogen-ion concentration probe by titration of known amounts of HCl with CO_2 -free NaOH solutions and by determining the equivalent point by Gran's method [46], which gives the standard potential, E° , and the ionic product of water ($pK_w = 13.83(1)$ in 0.1 M NMe_4Cl at 298.1 K). The stability constants were calculated from the potentiometric data by means of the computer program HYPERQUAD [47]. The concentration of HL was about 1×10^{-3} M in all experiments. The studied pH range was 2.0–11.5. Three measurements were performed and used to determine the protonation constants. Titration curves and relative fittings are reported in Figure S1.

2.6. Spectroscopic Measurements

UV-vis absorption spectra were recorded at 298 K by using a Jasco V-670 spectrophotometer (Jasco Europe, Lecco, Italy). Ligand solution was $[HL] = 2 \times 10^{-5}$ M. Spectra were recorded in the pH range 0.80–7.24 (a) and 7.24–12.58 (b). FT-IR spectra were recorded at room temperature on crystalline samples in attenuated total reflectance (ATR) mode with an IRAffinity-1S instrument (Shimadzu, Milan, Italy).

2.7. Single-Crystal X-ray Diffraction Analyses

Purple crystals of $HL \cdot EtOH \cdot H_2O$ and orange crystals of $H_3L(ReO_4)_2$ and $H_3L(ClO_4)_2 \cdot H_2O$ were used for X-ray diffraction analysis. A summary of the crystallographic data is reported in Table 1. The integrated intensities were corrected for Lorentz and polarization effects and an empirical absorption correction was applied [48]. The structures were solved by direct methods (SHELXS-97) [49]. Refinements were performed by means of full-matrix least-squares using SHELXL Version 2014/7 [50]. All non-hydrogen atoms were anisotropically refined. Hydrogen atoms were usually introduced in a calculated position and their coordinates were refined according to the linked atoms. Two different conformations were found for the nitroso group in the perrhenate salt. Their population parameters were refined constraining their sum to 1 (0.538/0.462 at the end of refinement). The acidic hydrogen atoms and one water hydrogen in $H_3L(ClO_4)_2 \cdot H_2O$ were localized in the Fourier difference maps, introduced in the calculation, and freely refined. In $H_3L(ReO_4)_2$, the acidic hydrogen atoms were introduced in the calculated position, linked to the pyridine nitrogens as found in the perchlorate salt, while in $HL \cdot EtOH \cdot H_2O$ both water hydrogen atoms were not localized in the Fourier difference map and not introduced in the calculation. The labeling schemes for anion complexes are reported in Figure S2. Selected H-bond contacts are listed in Table S1. CCDC numbers 2253138–2253140.

Table 1. Crystal data and structure refinement for HL·EtOH·H₂O, H₃L(ReO₄)₂, and H₃L(ClO₄)₂·H₂O.

	HL·EtOH·H ₂ O	H ₃ L(ReO ₄) ₂	H ₃ L(ClO ₄) ₂ ·H ₂ O
Empirical formula	C ₂₁ H ₃₀ N ₈ O ₄	C ₁₉ H ₂₄ N ₈ O ₁₀ Re ₂	C ₁₉ H ₂₆ Cl ₂ N ₈ O ₁₁
Formula weight	458.53	896.86	613.38
Temperature (K)	100(2)	100(2)	100(2)
space group	P-1	P2 ₁ /n	P2 ₁ /n
a (Å)	9.3960(4)	14.9381(9)	13.8500(5)
b (Å)	9.7782(4)	12.8194(6)	13.2210(5)
c (Å)	13.6308(6)	14.9659(7)	15.3154(6)
α (°)	76.058(2)	90	90
β (°)	70.650(2)	115.548(2)	113.661(2)
γ (°)	89.521(2)	90	90
Volume (Å ³)	1143.29(9)	2585.7(2)	2568.67(17)
Z	2	4	4
Independent reflections/R(int)	3500/0.1297	12,541/0.0662	4670/0.0583
μ (mm ⁻¹)	0.789/(Cu-kα)	9.423/(Mo-kα)	2.948/(Cu-kα)
R indices [I > 2σ(I)] *	R ₁ = 0.0546	R ₁ = 0.0639	R ₁ = 0.0851
	wR ₂ = 0.1759	wR ₂ = 0.1575	wR ₂ = 0.2241
R indices (all data) *	R ₁ = 0.1682	R ₁ = 0.0963	R ₁ = 0.0882
	wR ₂ = 0.2481	wR ₂ = 0.1802	wR ₂ = 0.2265

$$* R_1 = \sum ||F_o| - |F_c|| / \sum |F_o|; wR_2 = [\sum w(F_o^2 - F_c^2)^2 / \sum wF_o^4]^{1/2}.$$

2.8. Hirshfeld Surface Analysis

The Hirshfeld surface and the fingerprint plots were calculated using the Crystalexplorer17 software [51].

3. Results and Discussion

3.1. Ligand Protonation

The acid/base properties of HL were determined in order to know in which pH regions the different protonated forms of the receptor are formed and, thus, to be able to select the appropriate conditions for the synthesis of the anion complexes.

The analysis of the potentiometric titration curves, performed with the program HYPERQUAD [47], showed that HL undergoes one deprotonation in alkaline solutions and three protonations in acidic solutions: the corresponding equilibrium constants are reported in Table 2.

Table 2. Protonation constants determined in 0.1 M NMe₄Cl aqueous solution at 298.1 ± 0.1 K. Standard deviations are reported in parentheses.

Equilibrium	LogK
L ⁻ + H ⁺ = HL	11.88(1)
HL + H ⁺ = H ₂ L ⁺	5.82(3)
H ₂ L ⁺ + H ⁺ = H ₃ L ²⁺	3.04(3)
H ₃ L ²⁺ + H ⁺ = H ₄ L ³⁺	2.17(3)

In agreement with the behavior previously observed for other polyamines containing the same pyrimidine and pyridine groups [13,17,52–55], protonation occurring at high pH values (logK = 11.88, Table 2) is attributable to the secondary amine group, bound to the pyrimidine ring, which is deprotonated in very alkaline media, while protonation occurring in the lowest pH range (logK = 2.17, Table 2) is expected to involve the pyrimidine nitroso group (Scheme S1). The spectra of HL recorded in the near-UV at different pH values (Figure 2a,b) confirm this attribution of protonation sites. These spectra are characterized by three bands around 230, 257, and 330 nm which can be assigned to the allowed π–π* transitions between the π orbitals of the pyrimidine group and the overlap of the pyridine band at approximately 260 nm. As can be seen in Figure 2c, the pyrimidine bands undergo

important variation with pH in acidic (pH < 3) and alkaline (pH > 11.5) solutions when protonation involves the pyrimidine chromophore while the spectra are almost invariant in the intermediate region. This intermediate region is dominated by the presence of the HL and its monoprotonated H_2L^+ species (Figure 2). As the pyridine band at 260 nm is expected to increase upon protonation [56], the invariance of this band suggests that protonation of HL to give H_2L^+ occurs on the tertiary amine group (Scheme S1). Further protonation to form H_3L^{2+} necessarily involves a pyridine group and, indeed, the 260 nm band increases but the increase is accentuated by the almost concomitant formation of H_4L^{3+} in which, as already commented, the pyrimidine chromophore becomes protonated on the nitroso group.

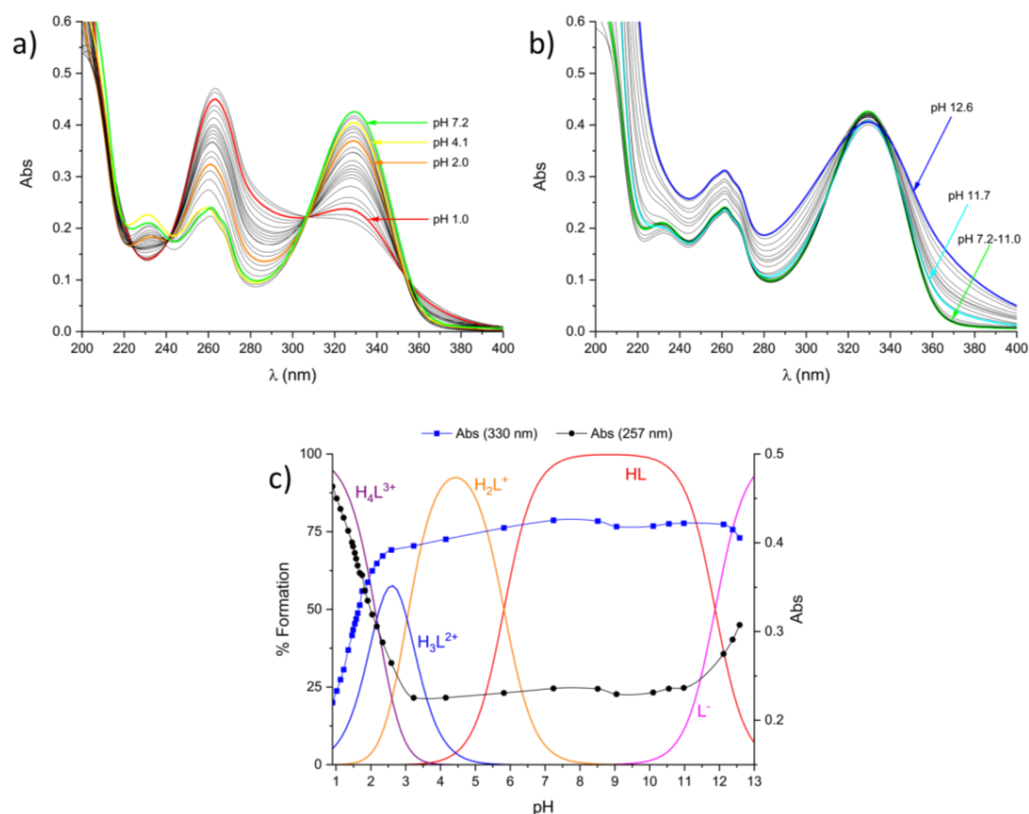


Figure 2. UV spectra of HL in the pH ranges 0.80–7.24 (a) and 7.24–12.58 (b). (c) Absorbances at 257 nm (●) and 330 nm (■) from the above spectra superimposed to the distribution diagram of the species formed by HL as a function of pH. $[HL] = 2 \times 10^{-5}$ M.

As for the location of the two ammonium groups in H_3L^{2+} , different alternatives should be considered: (i) one proton is located on the tertiary nitrogen atom (as in H_2L^+) and one on a pyridine; (ii) both pyridine groups are protonated; and (iii) protonation involves all three basic centers and there are several species in equilibrium with each other. The first alternative would be favored by the higher basicity of the tertiary amino group but could generate a strong repulsion between the neighboring ammonium groups, while, in the case of the second alternative, this electrostatic repulsion would be reduced since the two pyridines are the protonation sites which can stay at the maximum distance from each other. The third alternative would be a compromise between the first two. The crystal structures of perchlorate salt described below show that H_3L^{2+} contains two pyridinium groups, thus corroborating the second alternative (ii) (Scheme S1).

Based on the solution results, we decided to prepare the anion complexes at pH 2.5 in order to have in the solution the maximum abundance of the H_3L^{2+} species (Figure 2c). Although at such pH, H_2L^+ and H_4L^{3+} are also present in significant amounts, only

the $\text{H}_3\text{L}(\text{ReO}_4)_2$ and $\text{H}_3\text{L}(\text{ClO}_4)_2 \cdot \text{H}_2\text{O}$ salts were obtained and in fairly good yields (see Sections 2.3 and 2.4 above).

3.2. Crystallographic Study

3.2.1. Crystal Structure of $\text{HL} \cdot \text{EtOH} \cdot \text{H}_2\text{O}$

The crystal structure of the free ligand (HL), featuring co-crystallized ethanol and water molecules, is dominated by π - π stacking forces.

The arms of the tripodal ligand assume an overall Y conformation (Figure 3). One of the clefts of the ligand fully closes as one of the pyridine pendants gives face-to-face π - π stacking interaction with the nitroso-pyrimidine moiety (Figure 3, the dihedral angle between the rings' planes is 15.8 deg, the distance between ring centroids is 3.81 Å, and the shortest contact is $\text{C}2 \cdots \text{C}11$ 3.389(4) Å), resulting in a local U fold. Above and below, the same aromatic groups are involved in pyrimidine-pyrimidine (ring centroids distance 3.46 Å) or pyridine-pyridine (ring centroids distance 3.89 Å) π -stacking contacts connecting centrosymmetric molecules which stack upon each other forming columns (Figure 4).

As required by both intrinsic ring polarity and consequent space group symmetry, both pyridine-pyridine and pyrimidine-pyrimidine contacts feature the two neighboring rings in antiparallel disposition. Antiparallel stacks are then connected by $\text{NH}_2 \cdots \text{Nar}$ H-bonds ($\text{N}2 \cdots \text{N}7'$ 2.909(5) Å).

The second pyridine arm is not involved in face-to-face π - π stacking contacts, but it rather protrudes from, and panels, said stacked columns, being, moreover, involved in hydrogen bonding with solvent molecules. Beyond the $\text{N}8 \cdots \text{O}3'$ hydrogen bond (2.875(4) Å), neighboring hydrogen-bonded stacks interact with each other through further co-crystallized solvent-mediated ($\text{O}3 \cdots \text{O}4$ 2.735(4) Å) H-bonds, namely $\text{N}5 \cdots \text{O}3$ and $\text{O}4 \cdots \text{N}1'$ (2.791(3) Å and 2.963(4) Å, respectively (Figure S3, Table S1).

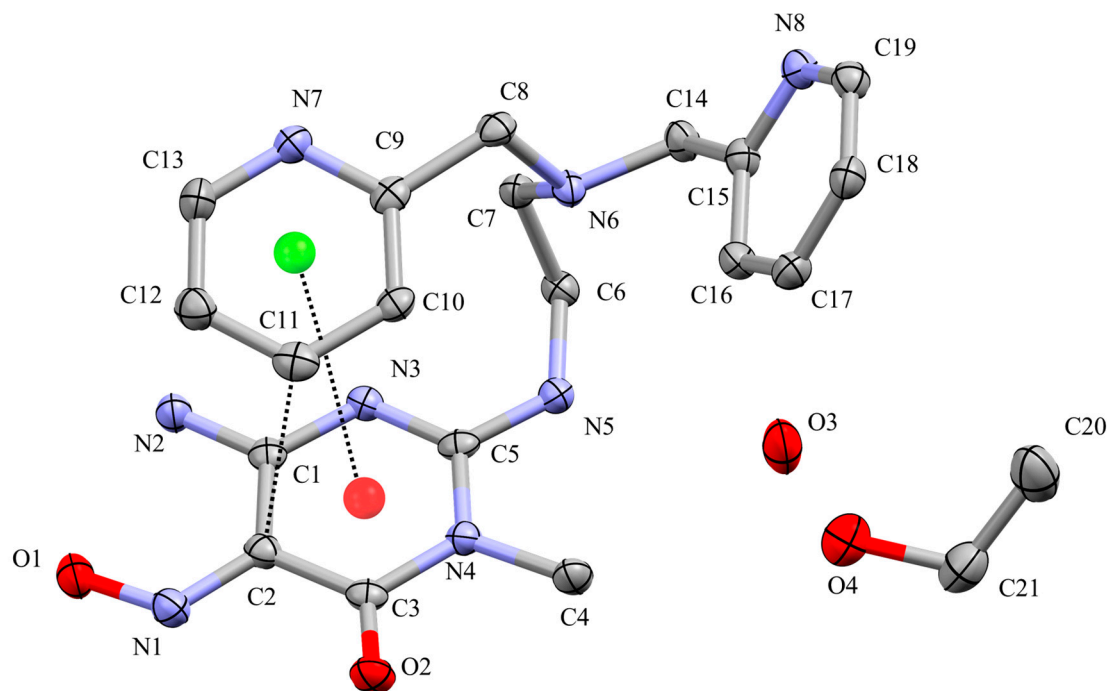


Figure 3. Asymmetric unit content of the $\text{HL} \cdot \text{EtOH} \cdot \text{H}_2\text{O}$ crystal structure with atom labeling.

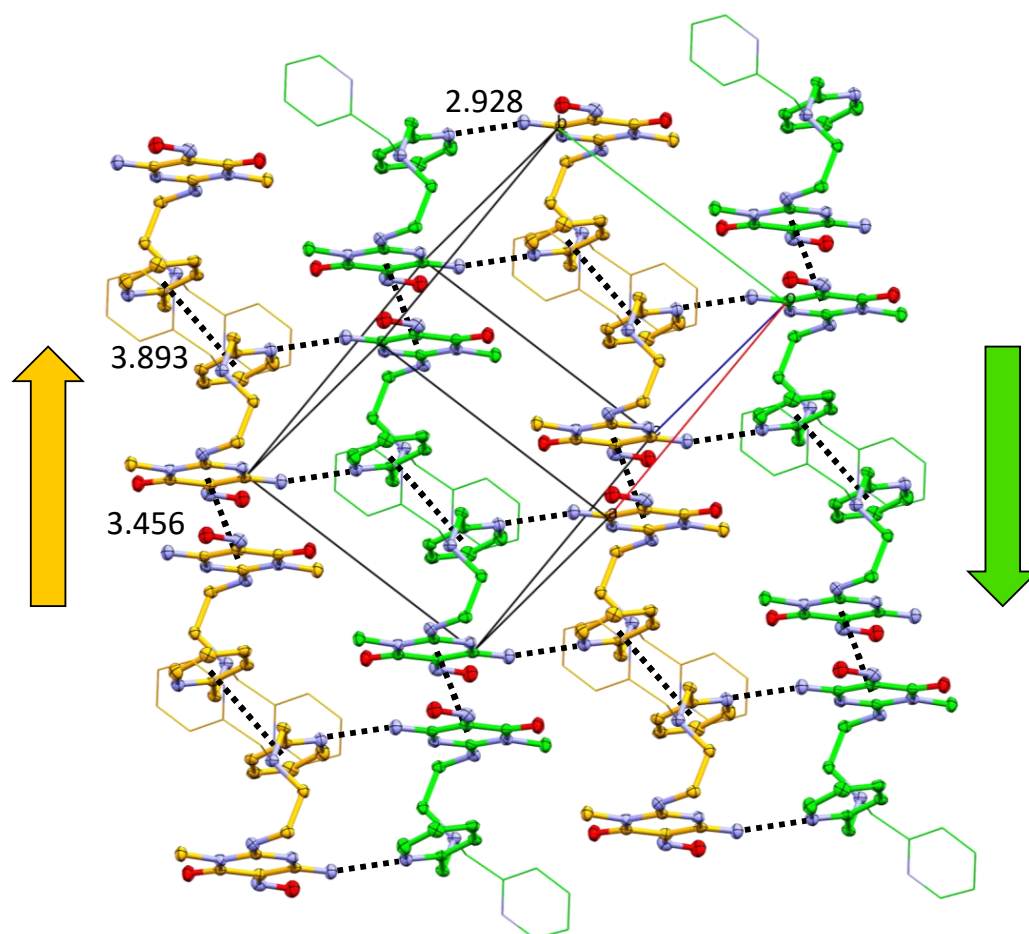


Figure 4. Repeats of antiparallel stacks of ligands (orange/green) featuring alternate head-to-tail pyridine/pyridine or pyrimidine/pyrimidine π - π stacking contacts in HL·EtOH·H₂O. H-bonded dimers alternate between inter- and intra-strand. The third arm of each ligand, not involved in strand formation, is shown as a wireframe. Hydrogen atoms and co-crystallized solvent molecules are omitted for clarity. Distances in Å.

3.2.2. Crystal Structures of the Anion Cleft Complexes H₃L(ReO₄)₂ and H₃L(ClO₄)₂·H₂O

The two structures can be considered isomorphous, having the same space group and almost the same cell parameters. The diprotonated ligand and the two anions (Figure 5) define very similar structural motifs: the U-shaped conformation seen for the not protonated ligand is now open and the three aromatic rings give two clamps gripping the two anions via anion- π interactions. The acidic hydrogens, which have been localized in the ΔF map for the perchlorate complex, are linked to both the pyridine nitrogen atoms, as expected from solution studies, and converge towards the nitroso oxygen of an adjacent symmetry-related ligand molecule (perchlorate complex: N7...O1 2.700(5) Å, N8...O1 2.793(6) Å; perrhenate complex: N7...O1 2.67(1) Å, N8...O1 2.62(1) Å, Table S1, see Figures S4 and S5 for the labeling scheme of both structures).

The pyrimidine-pyridine-pyridine ring sequence gives rise to the following dihedrals: 71.9/87.6 deg and 58.2/81.7 deg for the perchlorate and the perrhenate salt, respectively (Figure S6). Beyond these little differences, the ligand conformations are virtually identical (RMSD all atoms 0.2013), with their superposition, as shown in Figure 6, allowing us to discuss details of the anion-binding modes. The anion held by the pyridine-pyridine clamp has a very similar coordination mode, its central atom (Cl1 or Re2) being essentially located in the same position with respect to the ligand. These anions are equidistant from the two pyridine rings (Cl1 distance from pyridines centroids 4.089/4.108 Å, Re2 distance from pyridines centroids 4.172/3.958 Å) and give short contacts with the protonated nitrogen

atoms and with the neighboring aromatic carbon (shortest contacts range from 3.007(5) Å to 3.146(6) Å in the perchlorate salt and from 2.90(1) Å to 3.18(1) Å in the perrhenate salt).

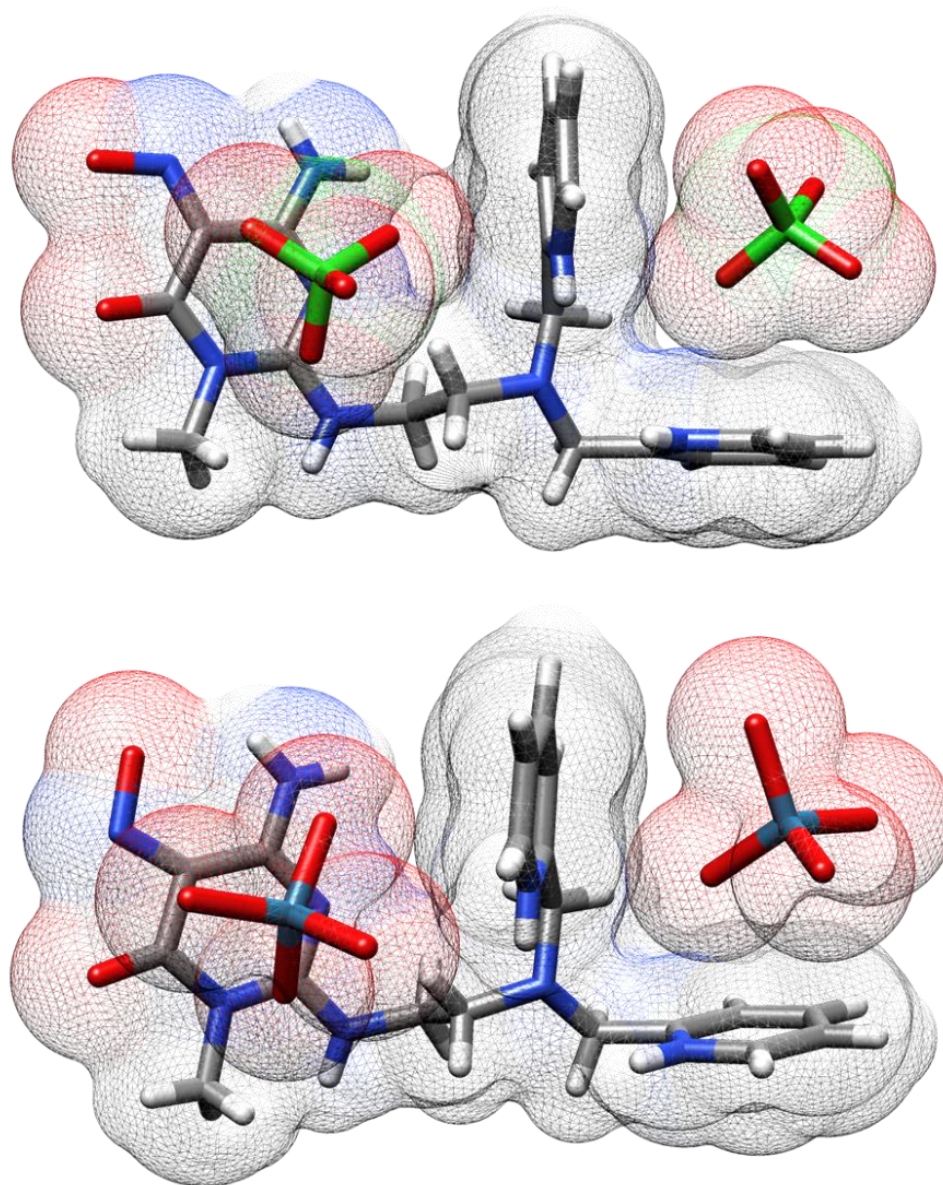


Figure 5. Synopsis of the perchlorate (**top**) and perrhenate (**bottom**) complexation inside the ligand clefts in the crystal structures of $\text{H}_3\text{L}(\text{ClO}_4)_2 \cdot \text{H}_2\text{O}$ and $\text{H}_3\text{L}(\text{ReO}_4)_2$.

The second cleft features two different aromatics, the polysubstituted pyrimidine being the most apt to anion– π binding. As a matter of fact, Cl2 perchlorate is closer to the pyrimidine ring ($\text{O}24 \cdots \text{N}4$ 2.977(4) Å, $\text{O}23 \cdots \text{C}2$ 3.290(6) Å) than to the pyridine ring ($\text{O}22 \cdots \text{N}7$ 3.123(6) Å), as expected (Figure S4). Instead, the Re1 perrhenate anion is almost equally distant from both rings ($\text{O}11 \cdots \text{C}13$ 3.18(1) Å, $\text{O}13 \cdots \text{N}4$ 3.169(9) Å, Figure S5). The mutual positions of these anions with respect to the ligand cleft is arguably the major difference between the two crystal structures, the difference being manifest in Figure 6. Such tuning of the ligand–anion interactions seem to stem from two other supramolecular forces at work, hydrogen bonding, and anion–anion contacts among perrhenate species, as shown in Figure 7.

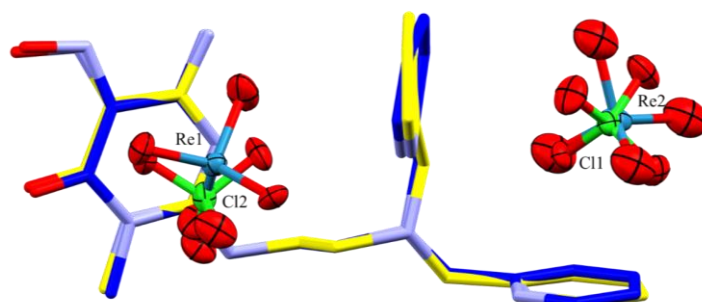


Figure 6. Superposition of the H_3L^{2+} cations found in the crystal structures of $\text{H}_3\text{L}(\text{ReO}_4)_2$ and $\text{H}_3\text{L}(\text{ClO}_4)_2 \cdot \text{H}_2\text{O}$ and differences in the relative positions of the anions inside the clefts.

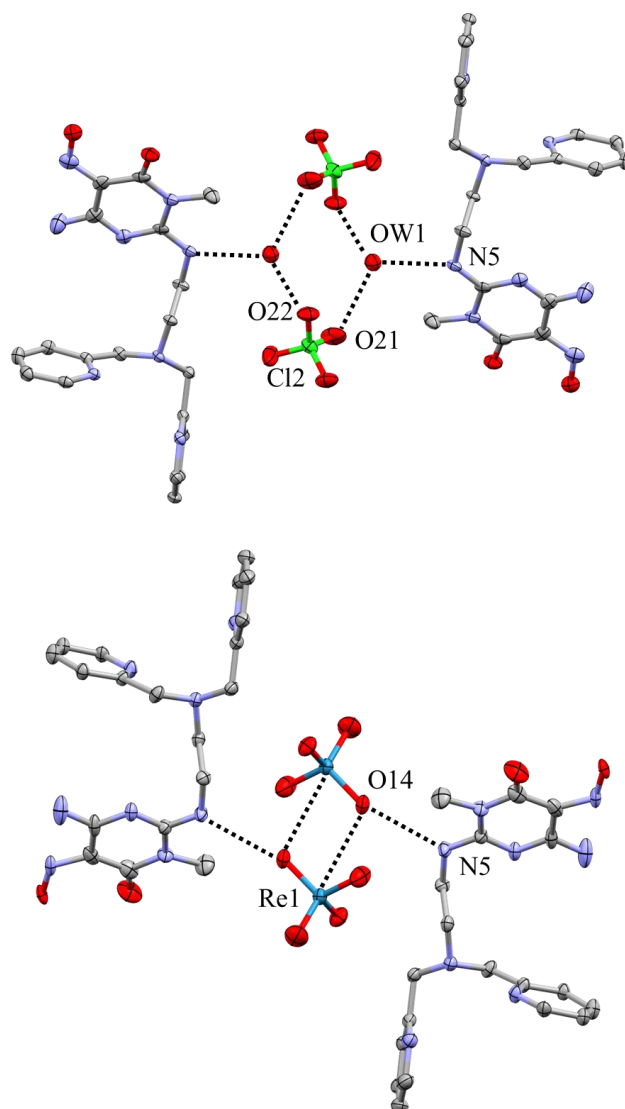


Figure 7. Details of further intermolecular contacts determining the exact disposition of anions bound within the pyrimidine–pyridine cleft in the crystal structures of $\text{H}_3\text{L}(\text{ClO}_4)_2 \cdot \text{H}_2\text{O}$ (above) and $\text{H}_3\text{L}(\text{ReO}_4)_2$ (below).

For both anions, the N5 nitrogen is involved in the binding. In the perrhenate case, this translates to a direct $\text{Re1}-\text{O14} \cdots \text{HN5}$ hydrogen bond ($\text{O} \cdots \text{N}$ distance 3.044(8) Å, Table S1). The same interaction in the monohydrate perchlorate complex is mediated by the solvent molecule, which also bridges two symmetry-related anions (H-bond distances: $\text{N5} \cdots \text{OW1}$ 2.756(6) Å, $\text{Cl2}-\text{O21} \cdots \text{OW1}$ 2.831(6) Å, $\text{OW1} \cdots \text{O22}-\text{Cl2}$ 2.885(5) Å, Table S1). Perrhenate

anions are also involved in weak mutual interactions with the establishment of a mutual $O\cdots Re/Re\cdots O$ contact ($O14\cdots Re1'$ 3.602(6) Å), which happens through one of the faces of the ReO_4^- tetrahedron. Similar contacts have been previously observed and recently dubbed *matere bonds* [57,58].

3.2.3. FT-IR Spectra Analysis

FT-IR spectra recorded on the crystalline samples of $HL\cdot EtOH\cdot H_2O$, $H_3L(ClO_4)_2\cdot H_2O$, and $H_3L(ReO_4)_2$ are shown in Figure S7. If we exclude the signals attributable to ethanol (900, 1157, 1219, 1238 cm^{-1}), which are present in the spectrum of $HL\cdot EtOH\cdot H_2O$, and some alteration of the relative intensity of the bands, the three spectra are essentially very similar, the main differences consisting in the presence of the typical bands of ClO_4^- (3361, 1065, 613 cm^{-1}) and ReO_4^- (895 cm^{-1}) [59]. The intense bands at 1065 cm^{-1} and 895 cm^{-1} due to the characteristic Cl-O and Re-O asymmetric stretching vibrations of ClO_4^- and ReO_4^- in the spectra of $H_3L(ClO_4)_2\cdot H_2O$ and $H_3L(ReO_4)_2$, respectively, are red-shifted as compared to spectra reported for $MClO_4$ (1076–1100 cm^{-1} , $M = Li^+, Na^+, NH_4^+$ [60–62]) and $MReO_4$ (913–928 cm^{-1} , $M = Na^+, K^+, NH_4^+$ [63,64]), manifesting the effect of anion complexation within the protonated ligand clefts.

3.2.4. Hirshfeld Surface Analysis

The Hirshfeld surface of the free ligand and corresponding fingerprint plot are reported in Figure 8.

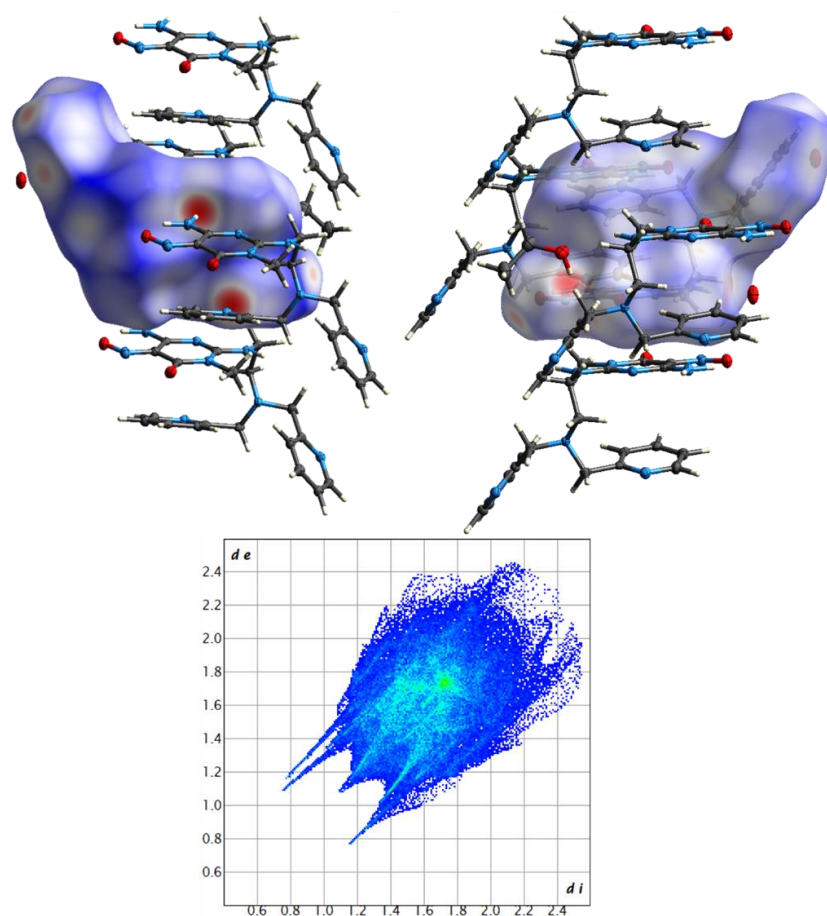


Figure 8. (Top): views of the HL Hirshfeld surface (d_{norm} coloring) in the $HL\cdot EtOH\cdot H_2O$ crystal structure. (Bottom): global fingerprint plot.

The Hirshfeld surface of HL is a rather flat block, delimited on top and bottom sides by intracolumn π - π stacking interactions and, on its sides, by intercolumn interactions, the most significant of which are the above-mentioned N2...N7 hydrogen bonds.

The fingerprint plot shows both typical H-bond tips and a manifest π - π stacking area (green portion of the graph centered at {1.7,1.7} coordinates). These are the same interaction types emerging from overall contact percentages (Table S2), with the further addition of H...O contacts due to hydrogen bonding to solvent molecules. The pseudosymmetry of the fingerprint graph is only slightly broken by the presence of the co-crystallized solvent molecules.

The Hirshfeld surface of the diprotonated ligand in the perchlorate and perrhenate complexes and corresponding fingerprint plots are shown in Figures 9 and 10, respectively.

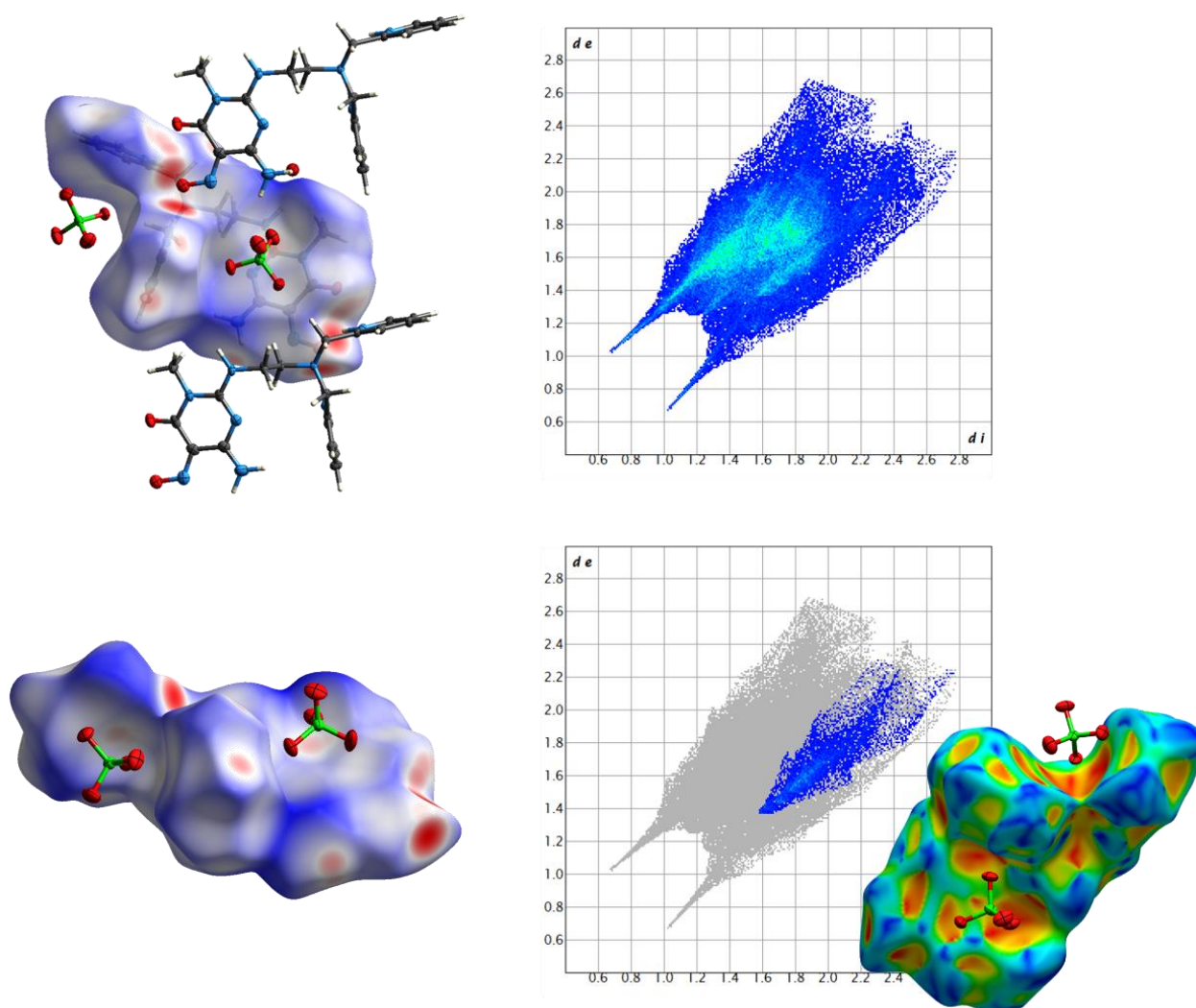


Figure 9. (Top): views of the H_3L^{2+} Hirshfeld surface (d_{norm} coloring) in the $H_3L(ClO_4)_2 \cdot H_2O$ crystal structure with main contacts highlighted and the full fingerprint plot. (Bottom): focus on the anion binding inside the clefts with detail of the C...O contact portion of the fingerprint plot. A shape index coloring scheme is also used to highlight the anion inclusion inside the binding pockets.

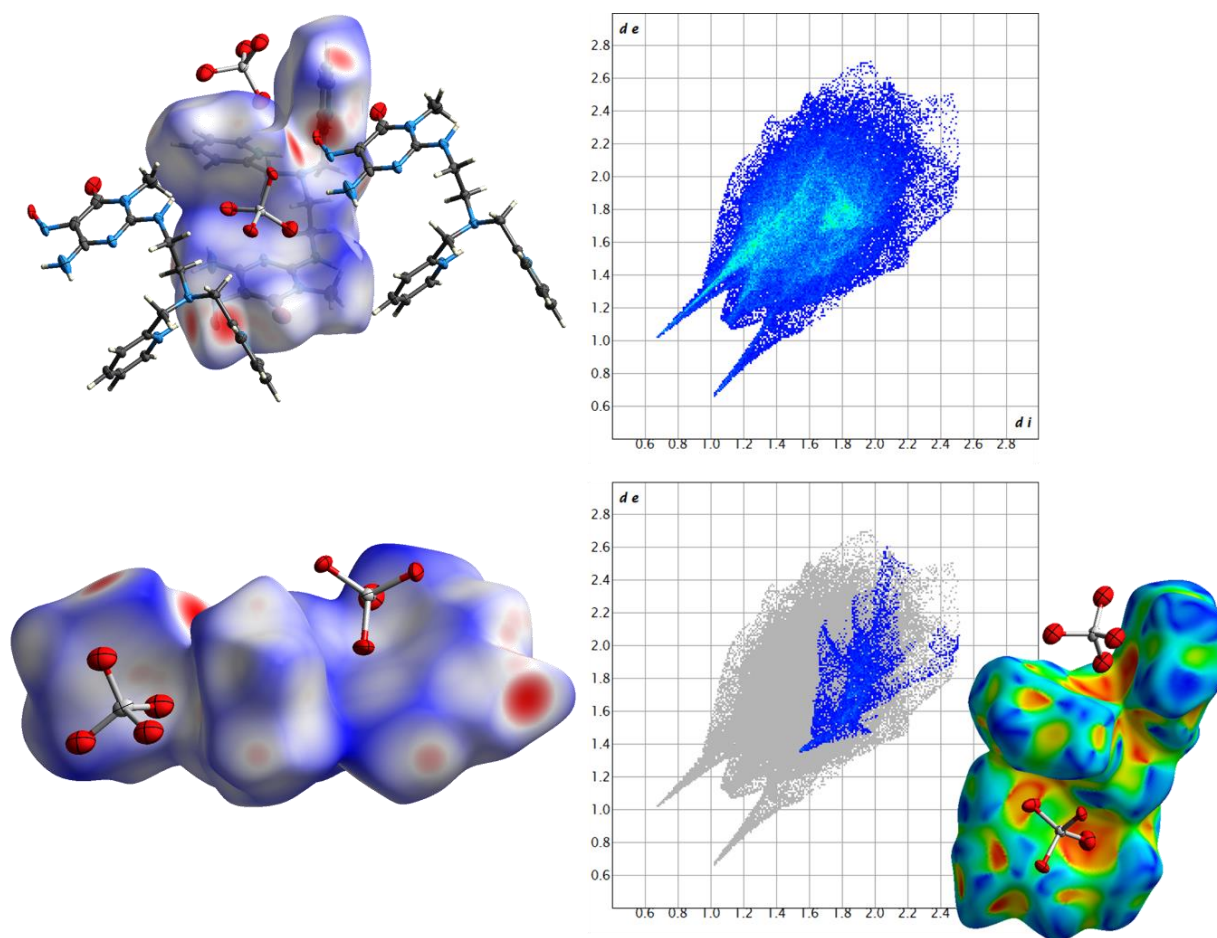


Figure 10. (Top): views of the H_3L^{2+} Hirshfeld surface (d_{norm} coloring) in the $H_3L(\text{ReO}_4)_2$ crystal structure with main contacts highlighted and the full fingerprint plot. (Bottom): focus on the anion binding inside the clefts with detail of the $C \cdots O$ contact portion of the fingerprint plot. A shape index coloring scheme is also used to highlight the anion inclusion inside the binding pockets.

Main interaction hotspots, as judged from the d_{norm} parameter, belong to the ligand–ligand H-bonds, namely among pyridinium sites and NO oxygen.

Anions are found in molecular clefts. The anion– π interaction is not as immediately manifest due to the simultaneous presence of H-bond type interactions, which, being both stronger and more directional, are easier to spot both from d_{norm} hotspots on the Hirshfeld surface and as sharp tips in the fingerprint plots. However, if $C \cdots O$, i.e., anion– π type contacts, are highlighted, the interaction is observed to be significantly represented in the fingerprint plot [22], and to account for a significant portion of the global Hirshfeld surface area (5.9% and 6.3% for ClO_4^- and ReO_4^- , respectively, Tables S3 and S4). The supramolecular hosting of anionic species is here perhaps better visualized through the shape index coloring, which is effective at showing inward/outward local bending of the Hirshfeld surface itself. As can be observed, anion-binding clefts are among the areas that show the most significant inward bending (red), signaling how the ligand’s surface engulfs the anions (Figures 9 and 10 bottom).

Of course, the contribution of these weak forces combines and synergizes with the electrostatic attraction generated between anions and ligands as a consequence of the positive charge introduced by protonation on the pyridine groups, which reverberates throughout the ring as evidenced by the calculated potential electrostatic surfaces (ESP) shown in Figure S8.

4. Conclusions

Tripodal ligands are convenient building blocks for easy and fast synthesis of efficient anion receptors. An example is given here by the HL ligand, characterized by a tren-like (tren = tris(2-aminoethyl)amine) structure bearing two pyridine and one pyrimidine terminal functionalities, whose synthesis was accomplished by means of a single reaction from commercial products. The crystal structure of the free ligand shows that the three arms decorated with aromatic groups define molecular clefts where host species can be included. Upon protonation, the ligand opens these clefts as wide as necessary for tight inclusion of large anions such as perchlorate and perrhenate, as shown in the solid state by the crystal structures of $\text{H}_3\text{L}(\text{ClO}_4)_2 \cdot \text{H}_2\text{O}$ and $\text{H}_3\text{L}(\text{ReO}_4)_2$. The ligand arms act as clamps gripping the two anions via anion– π interactions which are the main forces, in addition to the electrostatic attraction exerted by the ammonium groups that participate in strengthening the host–guest association. Intermolecular hydrogen bonding, π -stacking, and anion–anion interactions, in the case of perrhenate, contribute to stabilizing the crystal packing.

Supplementary Materials: The following supporting information can be downloaded at: <https://www.mdpi.com/article/10.3390/cryst13050823/s1>, Figure S1: Titration curves. Figure S2: Labelling schemes for anion complex structures. Figure S3: Pairs of hydrogen-bonded ligands (same color) joined in an H-bond network via co-crystallized solvent molecules. Figure S4: Selected short contacts (H-bonds and anion– π) in the perchlorate complex. Figure S5: Selected short contacts (H-bonds and anion– π) in the perrhenate complex. Figure S6: Details of the dihedral angles formed by the pyridine–pyridine–pyrimidine rings' sequence in the perchlorate and perrhenate salts. Figure S7: FT-IR spectra of crystalline $\text{HL} \cdot \text{EtOH} \cdot \text{H}_2\text{O}$, $\text{H}_3\text{L}(\text{ClO}_4)_2 \cdot \text{H}_2\text{O}$ and $\text{H}_3\text{L}(\text{ReO}_4)_2$. Figure S8: Electrostatic potential surfaces of HL and H_3L^{2+} . Scheme S1: Ligand protonation scheme. Table S1: Selected H-bond contacts. Table S2: Atoms in contact with the HL Hirshfeld surface in the $\text{HL} \cdot \text{EtOH} \cdot \text{H}_2\text{O}$ crystal structure. Table S3: Atoms in contact with the H_3L Hirshfeld surface in the $\text{H}_3\text{L}(\text{ClO}_4)_2 \cdot \text{H}_2\text{O}$ crystal structure. Table S4: Atoms in contact with the H_3L Hirshfeld surface in the $\text{H}_3\text{L}(\text{ReO}_4)_2$ crystal structure. Cif files of the three structures.

Author Contributions: Conceptualization, M.S., C.B. and A.B.; methodology, M.S., C.L. and C.B.; validation, M.S., C.B. and A.B.; investigation, C.C., C.L. and M.S.; data curation, C.C., C.L., M.S. and C.B.; writing—review and editing, M.S., C.B. and A.B.; funding acquisition, A.B. All authors have read and agreed to the published version of the manuscript.

Funding: This research received no external funding.

Data Availability Statement: Not applicable.

Acknowledgments: The financial support provided by the MUR—Dipartimenti di Eccellenza 2023–2027 (DICUS 2.0) to the Department of Chemistry “Ugo Schiff” of the University of Florence is acknowledged. This contribution is also based upon work from COST Action CA18202, NECTAR—Network for Equilibria and Chemical Thermodynamics Advanced Research, supported by COST (European Cooperation in Science and Technology).

Conflicts of Interest: The authors declare no conflict of interest.

References

1. Bianchi, A.; Bowman-James, K.; Garcia-España, E. (Eds.) *Supramolecular Chemistry of Anions*; Wiley-VCH: New York, NY, USA, 1997.
2. Sessler, J.L.; Gale, P.A.; Cho, W.S. *Anion Receptor Chemistry (Monographs in Supramolecular Chemistry)*; RSC Publishing: Cambridge, UK, 2006.
3. Bowman-James, K.; Bianchi, A.; Garcia-España, E. (Eds.) *Anion Coordination Chemistry*; Wiley-VCH: New York, NY, USA, 2012.
4. Zhao, J.; Yang, D.; Yang, X.-J.; Wu, B. Anion coordination chemistry: From recognition to supramolecular assembly. *Coord. Chem. Rev.* **2019**, *378*, 415–444. [[CrossRef](#)]
5. He, Q.; Tu, P.; Sessler, J.L. Supramolecular Chemistry of Anionic Dimers, Trimers, Tetramers, and Clusters. *Chem* **2018**, *4*, 46–93. [[CrossRef](#)] [[PubMed](#)]
6. Custelcean, R. Anion encapsulation and dynamics in self-assembled coordination cages. *Chem. Soc. Rev.* **2014**, *43*, 1813–1824. [[CrossRef](#)] [[PubMed](#)]

7. Bowman-James, K. Alfred Werner Revisited: The Coordination Chemistry of Anions. *Acc. Chem. Res.* **2005**, *38*, 671–678. [[CrossRef](#)]
8. Ilioudis, C.A.; Steed, J.W. Organic macrocyclic polyamine-based receptors for anions. *J. Supramol. Chem.* **2001**, *1*, 165–187. [[CrossRef](#)]
9. Llinares, J.M.; Powell, D.; Bowman-James, K. Ammonium based anion receptors. *Coord. Chem. Rev.* **2003**, *240*, 57–75. [[CrossRef](#)]
10. Gale, P.A. Anion receptor chemistry: Highlights from 1999. *Coord. Chem. Rev.* **2001**, *213*, 79–128. [[CrossRef](#)]
11. Dietrich, B. Design of anion receptors: Applications. *Pure Appl. Chem.* **1993**, *65*, 1457–1464. [[CrossRef](#)]
12. Bazzicalupi, C.; Bencini, A.; Bianchi, A.; Danesi, A.; Giorgi, C.; Valtancoli, B. Anion Binding by Protonated Forms of the Tripodal Ligand Tren. *Inorg. Chem.* **2009**, *48*, 2391–2398. [[CrossRef](#)]
13. García-Martín, J.; López-Garzón, R.; Godino-Salido, M.L.; Cuesta, R.; Gutiérrez-Valero, M.D.; Arranz-Mascarós, P.; Stoeckli-Evans, H. Adsorption of Zn²⁺ and Cd²⁺ from Aqueous Solution onto a Carbon Sorbent Containing a Pyrimidine–Polyamine Conjugate as Ion Receptor. *Eur. J. Inorg. Chem.* **2005**, *2005*, 3093–3103. [[CrossRef](#)]
14. Arranz, P.; Bianchi, A.; Cuesta, C.; Giorgi, C.; Godino, M.L.; Gutiérrez, M.D.; López, R.; Santiago, A. Binding and Removal of Sulfate, Phosphate, Arsenate, Tetrachloromercurate, and Chromate in Aqueous Solution by Means of an Activated Carbon Functionalized with a Pyrimidine-Based Anion Receptor (HL). Crystal Structures of [H₃L(HgCl₄)₃·H₂O and [H₃L(HgBr₄)₃·H₂O Showing Anion–π Interactions. *Inorg. Chem.* **2010**, *49*, 9321–9332.
15. Arranz, P.; Bazzicalupi, C.; Bianchi, A.; Giorgi, C.; Godino, M.L.; Gutiérrez, M.D.; López, R.; Savastano, M. Thermodynamics of Anion–π Interactions in Aqueous Solution. *J. Am. Chem. Soc.* **2013**, *135*, 102–105. [[CrossRef](#)] [[PubMed](#)]
16. Savastano, M.; Arranz, P.; Bazzicalupi, C.; Bianchi, A.; Giorgi, C.; Godino, M.L.; Gutiérrez, M.D.; López, R. Binding and removal of octahedral, tetrahedral, square planar and linear anions in water by means of activated carbon functionalized with a pyrimidine-based anion receptor. *RSC Adv.* **2014**, *4*, 58505–58513. [[CrossRef](#)]
17. Savastano, M.; Arranz-Mascarós, P.; Bazzicalupi, C.; Clares, M.P.; Godino-Salido, M.L.; Gutiérrez-Valero, M.D.; Guijarro, L.; Bianchi, A.; Garcia-España, E.; López-Garzón, R. Polyfunctional Tetraaza-Macrocyclic Ligands: Zn(II), Cu(II) Binding and Formation of Hybrid Materials with Multiwalled Carbon Nanotubes. *ACS Omega* **2017**, *2*, 3868–3877. [[CrossRef](#)] [[PubMed](#)]
18. Kou, X.; Ma, Y.; Pan, C.; Huang, Y.; Duan, Y.; Yang, Y. Effects of the Cationic Structure on the Adsorption Performance of Ionic Polymers toward Au(III): An Experimental and DFT Study. *Langmuir* **2022**, *38*, 6116–6127. [[CrossRef](#)] [[PubMed](#)]
19. Xu, Y.; Dang, D.; Zhang, N.; Zhang, J.; Xu, R.; Wang, Z.; Zhou, Y.; Zhang, H.; Liu, H.; Yang, Z.; et al. Aggregation-Induced Emission (AIE) in Superresolution Imaging: CXationic AIE Luminogens (AIEgens) for Tunable Organelle-Specific Imaging and Dynamic Tracking in Nanometer Scale. *ACS Nano* **2022**, *16*, 5932–5942. [[CrossRef](#)] [[PubMed](#)]
20. Das, A.; Sharma, P.; Frontera, A.; Verma, A.K.; Barcelo-Oliver, M.; Hussain, S.; Bhattacharyya, M.K. Energetically significant nitrile···nitrile and unconventional C–H···π(nitrile) interactions in pyridine based Ni(II) and Zn(II) coordination compounds: Antiproliferative evaluation and theoretical studies. *J. Mol. Struct.* **2021**, *1223*, 129246. [[CrossRef](#)]
21. Qi, B.; An, S.; Luo, J.; Liu, T.; Song, Y.-F. Enhanced Macroanion Recognition of Superchaotropic Keggin Clusters Achieved by Synergy of Anion–π and Anion–Cation Interactions. *Chem. Eur. J.* **2020**, *26*, 16802–16810. [[CrossRef](#)]
22. Martínez-Camarena, Á.; Savastano, M.; Bazzicalupi, C.; Bianchi, A.; García-España, E. Stabilisation of Exotic Tribromide (Br₃[−]) Anions via Supramolecular Interaction with a Tosylated Macrocyclic Pyridinophane. A Serendipitous Case. *Molecules* **2020**, *25*, 3155. [[CrossRef](#)]
23. Savastano, M.; Bazzicalupi, C.; Gellini, C.; Bianchi, A. Infinite supramolecular pseudo-polyrotaxane with poly[3]catenane axle: Assembling nanosized rings from mono- and diatomic I[−] and I₂ tectons. *Chem. Commun.* **2020**, *56*, 551–554. [[CrossRef](#)]
24. Savastano, M.; Bazzicalupi, C.; Gellini, C.; Bianchi, A. Genesis of complex polyiodide networks: Insights on the blue box/I[−]/I₂ ternary system. *Crystals* **2020**, *10*, 387. [[CrossRef](#)]
25. Savastano, M.; Bazzicalupi, C.; Bianchi, A. Porous frameworks based on supramolecular ball joints: Bringing flexibility to ordered 3D lattices. *Chem. Eur. J.* **2020**, *26*, 5994–6005. [[CrossRef](#)] [[PubMed](#)]
26. Giese, M.; Albrecht, M.; Repenko, T.; Sackmann, J.; Valkonen, A.; Rissanen, K. Single-Crystal X-ray Diffraction and Solution Studies of Anion–π Interactions in N-(Pentafluorobenzyl)pyridinium Salts. *Eur. J. Org. Chem.* **2014**, *2014*, 2435–2442. [[CrossRef](#)]
27. Biswas, C.; Drew, M.G.B.; Escudero, D.; Frontera, A.; Ghosh, A. Anion–π, Lone-Pair–π, π–π and Hydrogen-Bonding Interactions in a Cu^{II} Complex of 2-Picolinate and Protonated 4,4′-Bipyridine: Crystal Structure and Theoretical Studies. *Eur. J. Inorg. Chem.* **2009**, *2009*, 2238–2246. [[CrossRef](#)]
28. de Hoog, P.; Gamez, P.; Mutikainen, I.; Turpeinen, U.; Reedijk, J. An Aromatic Anion Receptor: Anion–p Interactions do Exist. *Angew. Chem. Int. Ed.* **2004**, *43*, 5815–5817. [[CrossRef](#)]
29. Krishnan Suresh, K.; Subbiah, K.; Kalivel, P.; Ayyasamy, S.; Palanivel, S. Environmental occurrence, toxicity and remediation of perchlorate—A review. *Chemosphere* **2023**, *311*, 137017.
30. Shukla, M.K.; Boddu, V.M.; Steevens, J.A.; Damavarapu, R.; Leszczynski, J. (Eds.) *Energetic Materials: From Cradle to Grave. In Challenges and Advances in Computational Chemistry and Physics*; Springer: Berlin/Heidelberg, Germany, 2018; Volume 25.
31. Vogt, H.; Balej, J.; Bennett, J.E.; Wintzer, P.; Sheikh, S.A.; Gallone, P. Chlorine Oxides and Chlorine Oxygen Acids. In *Ullmann's Encyclopedia of Industrial Chemistry*; Wiley-VCH: New York, NY, USA, 2002.
32. Gu, B.; Coates, J.D. (Eds.) *Perchlorate. Environmental Occurrence, Interactions and Treatment*; Springer Nature: Berlin/Heidelberg, Germany, 2006.

33. Da, H.-J.; Yang, C.-X.; Yan, X.-P. Cationic Covalent Organic Nanosheets for Rapid and Selective Capture of Perrhenate: An Analogue of Radioactive Pertechnetate from Aqueous Solution. *Environ. Sci. Technol.* **2019**, *53*, 5212–5220. [CrossRef]
34. Kohlickova, M.; Jedinakova-Krizova, V.; Melichar, F. Rhenium complexes in nuclear medicine. *Chem. Listy* **2000**, *94*, 151–158.
35. Volkert, W.A.; Hoffman, T.J. Therapeutic Radiopharmaceuticals. *Chem. Rev.* **1999**, *99*, 2269–2292. [CrossRef]
36. Colton, R. *The Chemistry of Rhenium and Technetium*, 1st ed.; John Wiley and Sons Ltd.: Hoboken, NJ, USA; Interscience Publishers: New York, NY, USA, 1965.
37. Banerjee, D.; Kim, D.; Schweiger, M.J.; Krugerc, A.A.; Thallapally, P.K. Removal of TcO_4^- ions from solution: Materials and future outlook. *Chem. Soc. Rev.* **2016**, *45*, 2724–2739. [CrossRef]
38. Katayev, E.A.; Kolesnikov, G.V.; Sessler, J.L. Molecular recognition of pertechnetate and perrhenate. *Chem. Soc. Rev.* **2009**, *38*, 1572–1586. [CrossRef] [PubMed]
39. Gale, P.A.; Howe, N.W.; Wu, X. Anion Receptor Chemistry. *Chem* **2016**, *1*, 351–422. [CrossRef]
40. Zhou, W.; Li, A.; Gale, P.A.; He, Q. A highly selective superphane for ReO_4^- recognition and extraction. *Cell Rep. Phys. Sci.* **2022**, *3*, 100875. [CrossRef]
41. Macreadie, L.K.; Gilchrist, A.M.; McNaughton, D.A.; Ryder, W.G.; Fares, M.; Gale, P.A. Progress in anion receptor chemistry. *Chem* **2022**, *8*, 46–118. [CrossRef]
42. Low, N.J.; López, M.D.; Arranz, P.; Cobo, J.; Godino, M.L.; López, R.; Gutiérrez, M.D.; Melguizo, M.; Ferguson, G.; Glidewell, C. N-(6-Amino-3,4-dihydro-3-methyl-5-nitroso-4-oxopyrimidin-2-yl) derivatives of glycine, valine, serine, threonine and methionine: Interplay of molecular, molecular-electronic and supramolecular structures. *Acta Cryst. B* **2000**, *56*, 882–892. [CrossRef]
43. Bazzicalupi, C.; Bianchi, A.; Biver, T.; Giorgi, C.; Santarelli, S.; Savastano, M. Formation of double-strand dimetallic helicates with a terpyridine-based macrocycle. *Inorg. Chem.* **2014**, *53*, 12215–12224. [CrossRef]
44. Fontanelli, M.; Micheloni, M. *Proceedings of the I Spanish-Italian Congress on Thermodynamics of Metal Complexes*; Diputación de Castellón: Castellón, Spain, 1990; pp. 41–43.
45. Savastano, M.; Fiaschi, M.; Ferraro, G.; Gratteri, P.; Mariani, P.; Bianchi, A.; Bazzicalupi, C. Sensing Zn^{2+} in Aqueous Solution with a Fluorescent Scorpion Macrocyclic Ligand Decorated with an Anthracene Bearing Tail. *Molecules* **2020**, *25*, 1355. [CrossRef]
46. Gran, G. Determination of the equivalence point in potentiometric titrations. Part II. *Analyst* **1952**, *77*, 661–671. [CrossRef]
47. Gans, P.; Sabatini, A.; Vacca, A. Investigation of equilibria in solution. Determination of equilibrium constants with the HYPERQUAD suite of programs. *Talanta* **1996**, *43*, 1739–1753. [CrossRef]
48. Krause, L.; Herbst-Irmer, R.; Sheldrick, G.M.; Stalke, D. Comparison of silver and molybdenum microfocus X-ray sources for single-crystal structure determination. *J. Appl. Cryst.* **2015**, *48*, 3–10. [CrossRef]
49. Sheldrick, G.M. A short history of SHELX. *Acta Crystallogr. A* **2008**, *64*, 112–122. [CrossRef] [PubMed]
50. Sheldrick, G.M. Crystal structure refinement with SHELXL. *Acta Cryst.* **2015**, *C71*, 3–8.
51. Turner, M.J.; McKinnon, J.J.; Wolff, S.K.; Grimwood, D.J.; Spackman, P.R.; Jayatilaka, D.; Spackman, M.A. *CrystalExplorer17*; University of Western Australia: Crawley, WA, Australia, 2017; Available online: <https://crystalexplorer.net> (accessed on 6 February 2023).
52. Savastano, M.; Arranz-Mascarós, P.; Clares, M.P.; Cuesta, R.; Godino-Salido, M.L.; Guijarro, L.; Gutiérrez-Valero, M.D.; Inclán, M.; Bianchi, A.; García-España, E.; et al. A new heterogeneous catalyst obtained via supramolecular decoration of graphene with a Pd^{2+} azamacrocyclic complex. *Molecules* **2019**, *24*, 2714. [CrossRef] [PubMed]
53. Savastano, M.; Arranz-Mascarós, P.; Bazzicalupi, C.; Clares, M.P.; Godino-Salido, M.L.; Gutiérrez-Valero, M.D.; Inclán, M.; Bianchi, A.; García-España, E.; López-Garzón, R. Construction of green nanostructured heterogeneous catalysts via non-covalent surface decoration of multi-walled carbon nanotubes with Pd(II) complexes of azamacrocycles. *J. Catal.* **2017**, *353*, 239–249. [CrossRef]
54. Godino-Salido, M.-L.; Santiago-Medina, A.; Arranz-Mascarós, P.; López-Garzón, R.; Gutiérrez-Valero, M.D.; Melguizo, M.; López-Garzón, F.J. Novel active carbon/crown ether derivative hybrid material for the selective removal of Cu(II) ions: The crucial role of the surface chemical functions. *Chem. Eng. Sci.* **2014**, *114*, 94–104. [CrossRef]
55. Savastano, M.; Passaponti, M.; Giurlani, W.; Lari, L.; Bianchi, A.; Innocenti, M. Multi-Walled Carbon Nanotubes Supported Pd(II) Complexes: A Supramolecular Approach towards Single-Ion Oxygen Reduction Reaction Catalysts. *Energies* **2020**, *13*, 5539. [CrossRef]
56. Hughes, E.B.; Jellinek, H.H.G.; Ambrose, B.A. Pyridine. Ultraviolet Absorption Spectrum and Dissociation Constant. *J. Phys. Chem.* **1949**, *53*, 410–414. [CrossRef]
57. Daolio, A.; Pizzi, A.; Terraneo, G.; Frontera, A.; Resnati, G. Anion···Anion Interaction involving σ -Holes of Perrhenate, Pertechnetate and Permanganate Anions. *ChemPhysChem* **2021**, *22*, 2281–2285. [CrossRef]
58. Gomila, R.M.; Frontera, A. Matere Bonds vs. Multivalent Halogen and Chalcogen Bonds: Three Case Studies. *Molecules* **2022**, *27*, 6597. [CrossRef]
59. Nyquist, R.A.; Kagel, R.O. *Infrared and Raman Spectra of Inorganic Compounds and Organic Salts*, 2nd ed.; Academic Press: New York, NY, USA, 1971.
60. Sima, L.H.; Ganb, S.N.; Chana, C.H.; Yahyab, R. ATR-FTIR studies on ion interaction of lithium perchlorate in polyacrylate/poly(ethylene oxide) blends. *Spectrochim. Acta Part A* **2010**, *76*, 287–292. [CrossRef]
61. Chandrawanshi, S.; Verma, S.K.; Deb, M.K. Collective Ion-Pair Single-Drop Microextraction Attenuated Total Reflectance Fourier Transform Infrared Spectroscopic Determination of Perchlorate in Bioenvironmental Samples. *J. AOAC Int.* **2018**, *101*, 1145–1155. [CrossRef] [PubMed]

62. Hori, K.; Iwama, A.; Fukuda, T. FTIR Spectroscopic Study on the Interaction between Ammonium Perchlorate and Bonding Agents. *Propell. Explos. Pyrot.* **1990**, *15*, 99–102. [[CrossRef](#)]
63. Gonzalez-Rodriguez, J.; Pepper, K.; Baron, M.G.; Mamo, S.K.; Simons, A.M. Production and Analysis of Recycled Ammonium Perrhenate from CMSX-4 superalloys. *Open Chem.* **2018**, *16*, 1298–1306. [[CrossRef](#)]
64. Gassman, P.-L.; McCloy, J.S.; Soderquist, C.Z.; Schweiger, M.J. Raman analysis of perrhenate and pertechnetate in alkali salts and borosilicate glasses. *J. Raman Spectrosc.* **2014**, *45*, 139–147. [[CrossRef](#)]

Disclaimer/Publisher's Note: The statements, opinions and data contained in all publications are solely those of the individual author(s) and contributor(s) and not of MDPI and/or the editor(s). MDPI and/or the editor(s) disclaim responsibility for any injury to people or property resulting from any ideas, methods, instructions or products referred to in the content.